Hindawi
Adsorption Science & Technology
Volume 2021, Article ID 5540517, 14 pages
https://doi.org/10.1155/2021/5540517

Research Article

Statistical Physics Modeling of Sorption Isotherms of Aluminum, Iron, and Indium on Tetraphenylporphyrin (H_2TPP) and Tetrakis(4-tolylphenyl)porphyrin (H_2TTPP): Phenomenological Investigation of Metalloporphyrins at the Molecular Level

Zainab Elqahtani,[1] Mohamed Ben Yahia,[2] Nada Alfryyan,[1] Shatha Aldaghfag,[1] and Fatma Aouaini[1]

[1]*Department of Physics, College of Science, Princess Nourah Bint Abdulrahman University, Riyadh, Saudi Arabia*
[2]*Laboratory of Quantum and Statistical Physics LR18ES18, Faculty of Sciences of Monastir, Monastir 5000, Tunisia*

Correspondence should be addressed to Mohamed Ben Yahia; ben_yahia_med@hotmail.fr
and Fatma Aouaini; aouainif@yahoo.com

Received 8 January 2021; Revised 6 March 2021; Accepted 31 March 2021; Published 21 April 2021

Academic Editor: Senthil Kumar Ponnusamy

A quartz crystal adsorbent functionalized with two promising porphyrins (the 5,10,15,20-tetrakis(4-tolylphenyl)porphyrin and the 5,10,15,20-tetraphenylporphyrin) was applied for the investigation of the adsorption phenomenon of aluminum chloride, iron chloride, and indium chloride. The aim is to prove new insights about the appropriate adsorption materials for metalloporphyrin fabrication. The equilibrium isotherms were measured at five adsorption temperatures (from 290 to 330 K) through the microbalance (QCM) method. The discussion of the experimental observations indicated that the adsorption of the aluminum chloride and the iron chloride was performed via a monolayer process. On contrary, the participation of the chloride ions in the double-layer adsorption of the indium chloride was explained by the layer-by-layer process. Overall, the statistical physics modeling of the experimental curves indicated that the number of ions per adsorbent site n was found inferior to 1 for all the adsorption systems (multi-interaction process for the three ions). Interestingly, the physicochemical investigation of the three adopted models showed that the complexation mechanism of the tested porphyrins was an endothermic process since the two steric parameters (n and P_M) increased with the rise of the temperature. The $FeCl_3$ curves were discussed via a monolayer adsorption model which includes the parameters a and b (lateral interaction description), indicating the lowest stability of the formed iron-porphyrin complex. The energetic study showed that the adsorption energies $|-\Delta E_{1/2}|$ of $AlCl_3$ on H_2TTPP and H_2TPP are superior to 40 kJ/mol (chemical adsorption mechanism), whereas the adsorption mechanisms of $FeCl_3$ and $InCl_3$ took place via a physical process since they presented adsorption energy values lower than 40 kJ/mol.

1. Introduction

In recent years, porphyrins have been studied as chemical sensor materials of various metals leading to the formation of metalloporphyrin complexes [1, 2]. The metal-porphyrin complexes have received increased interest in several biological and environmental processes such as stereochemistry study and molecular recognition [3–6]. Note here that the nature of the central ion has influenced the photophysical properties of porphyrins [7, 8]. For example, these tetrapyrrolic macrocycles are involved in the chlorophyll structure (magnesium-porphyrin complex) and the hemoglobin structure (iron-porphyrin complex), so they are known as pigments of life [8]. In addition, metalloporphyrin complexes were also used as ionophores in the development of potentiometric recognition sensors supported with their structural

variety and coordination chemistry [7, 8]. In particular, the photosensitizing properties of aluminum(III)-porphyrin have promoted its use as potential ionophore of fluoride [9, 10]. Moreover, the aluminum(III)-porphyrin and the indium(III)-porphyrin have been potentially used as supramolecular building blocks [11] and numerous other areas (sensing, molecular recognition, polymerisation reactions, etc.) [12, 13]. Surprisingly, it was remarked that while several papers have been devoted to metalloporphyrin complexes including the metal centers zinc, rhodium, and cobalt [14, 15], little attention has been paid to the use of porphyrins as complexing compounds of aluminum(III), iron(III), and indium(III) (Figure 1) despite their contribution in the interesting fields indicated above. In fact, the adsorption of these three metals on two tested porphyrins (H_2TPP and H_2TTPP) was examined in the present investigation.

In the literature, many approaches have been applied for the investigation of the adsorption mechanism of metals such as the sorption/reduction of heavy metal ions in environmental pollution management [16, 17]. Other experimental methods have been applied for the investigation of the adsorption mechanism [18–20], but in this work, the adsorption mechanisms of aluminum chloride, iron chloride, and indium chloride have been investigated by the QCM technique for many reasons. Firstly, this experimental method is a simple mass detector technique which requires the immobilization of porphyrins on the solid support of the quartz crystal. Then, the complexed mass of the metal into the macromolecule cavities can be controlled through the microbalance apparatus. Secondly, the metal-porphyrin complexes do not require an inert environment, and they are stable in the presence of water. Thirdly, the use of the QCM technique enables to plot the adsorption curves which describe the complexed amount of metallic ions on porphyrins at different temperatures. Lastly, the microscopic characteristics of the resulting film can be followed by easily fitting the experimental isotherms with analytical models [21].

According to the literature, the physical models were adopted by numerous authors to examine the adsorption problem. For example, the empirical expressions of the Langmuir and Freundlich models [22, 23] have been applied for the description of the isotherm curves, but they did not give a deep physicochemical analysis of the adsorption process. Importantly, the analytical adsorption models of the present investigation were established through the innovative statistical physics theory [24, 25] which provides the new vision about the metalloporphyrin description. Based on this idea, the fundamental aim of the modeling work of adsorption isotherms is to find the sufficient systematic model that can anticipate physical insights of porphyrin adsorption based on the physicochemical parameters of the statistical physics models [26].

2. Experimental Adsorption Isotherms

2.1. Materials. The aluminum(III) chloride ($AlCl_3$), the iron(III) chloride ($FeCl_3$), and the indium(III) chloride ($InCl_3$) are the tested adsorbates in this paper.

The tetrakis(4-tolylphenyl)porphyrin (H_2TTPP) and the tetraphenylporphyrin (H_2TPP) are the porphyrins used in these experiments. They were synthesized based on a published method (the Adler-Longo strategy) [27].

Figure 2 shows the synthesis methods of porphyrins H_2TPP and H_2TTPP.

H_2TPP (Figure 2(a)) was synthesized through the reaction between propanoic acid (2 L) and benzaldehyde (40 mL). The synthesis of H_2TTPP (Figure 2(b)) was performed by introducing 4-tolualdehyde (12.5 g) with the propanoic acid (110 mL). Note that the synthesis of the two tested adsorbents has been performed by following the same procedure (reflux for 30 min, allowing for cooling, filtration, and drying under vacuum for 3 hours). The dried solid mass of H_2TPP was 9.76 g while the obtained mass of H_2TTPP was 3 g. The two solid compounds of porphyrins were dissolved in chloroform giving two solutions with concentration of $2.9\ 10^{-2}\ \text{mol}\cdot\text{L}^{-1}$.

2.2. Experimental Measurements. The experimental QCM setup is presented in Figure 3.

The QCM measurements were performed based on the piezoelectric quartz crystal [28, 29]. The crystal is a thin disc which is cut from the polished quartz (AT-cut). The fundamental resonant frequency of the quartz is 5 MHz, and the diameter of the disc is 2.54 cm [29]. A cleaning treatment was applied on the crystals by means of a Piranha solution at room temperature followed with rinsing with ethanol and drying with high purity nitrogen.

For the adsorption measurement, 60 μL of the adsorbents (porphyrins H_2TPP and H_2TTPP) was doped onto the clean crystal surface by the spin coating technique at 3500 rpm for 30 seconds. The functionalized crystals were dried at 393 K for 2 hours.

The functionalized crystal (adsorption cell) was placed in a Teflon probe, which was covered by a protective ring, and it was immersed in $V_s = 100$ mL of pure water contained in the bain-marie. The stabilization of the resonant frequency in the reactor took about 1 hour, and we noted the crystal frequency F_0 after the stabilization. Then, we proceed with the injection of volumes of stock solutions of the adsorbates ($AlCl_3$/$FeCl_3$/$InCl_3$) in the reactor. The added volumes of adsorbates V_{ad} should be calculated according to the next equation:

$$V_{ad} = \frac{c_f \times V_s}{c_0}, \tag{1}$$

where V_s is the initial volume in the reactor, c_0 is the concentration of the prepared adsorbate solution, and c_f is the final concentration in the reactor.

At least 15 injections into the reactor were performed using a micropipette, then the variation of the resonant frequency (corresponding to the new adsorbate concentration in the reactor) was determined as follows:

$$\Delta f = F_i - F_0. \tag{2}$$

with F_i as the resonant frequency after each adsorbate injection and F_0 characterizing the effect of the hydrostatic

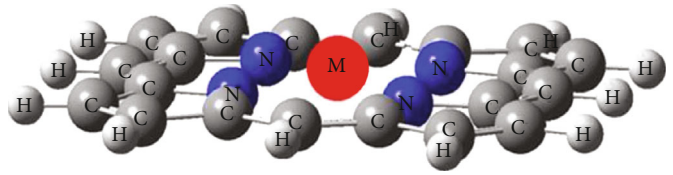

Figure 1: Chemical structure of the metalloporphyrin complexes.

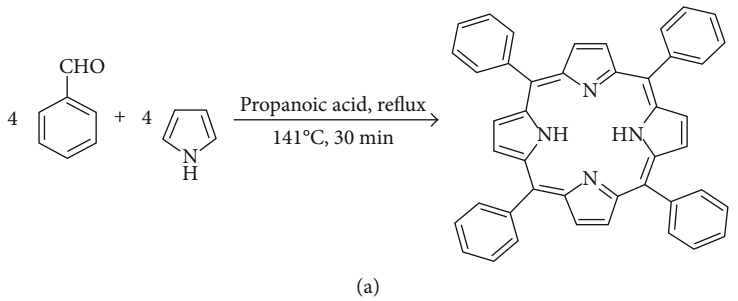

Figure 2: Synthesis methods of the 5,10,15,20-tetraphenylporphyrin (H_2TPP) and the 5,10,15,20-tetrakis(4-tolylphenyl)porphyrin (H_2TTPP).

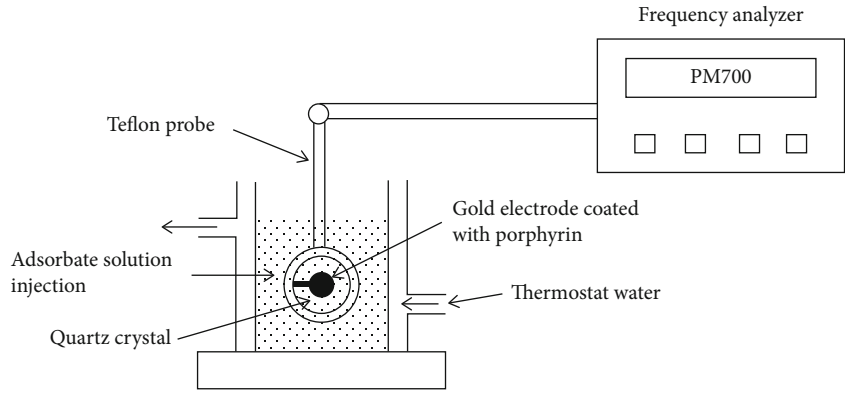

Figure 3: Experimental setup of the quartz crystal microbalance.

pressure on the quartz crystal. It can be understood from this equation that the frequency variation Δf is only the result of the mass variation Δm of the metal on the porphyrin surface and does not consider any effect from the quartz crystal on the adsorption process since the hydrostatic pressure effect on the quartz (frequency F_0) is not considered in the measured frequency variation Δf.

2.3. Sauerbrey's Equation. The deposited mass of the metallic ions on the surface after each injection was determined according to the Sauerbrey hypothesis which links the mass variation to the frequency change [30–32]:

$$\Delta f = -C \times \Delta m, \tag{3}$$

where C is the crystal sensitivity factor ($\mathrm{Hz{\cdot}cm^2{\cdot}\mu g^{-1}}$). Here, keep in mind that this relation should be applied when the resonant frequency variation is mainly due to the change of the deposited mass on the adsorption surface.

In order to justify the application of the Sauerbrey equation in a liquid medium, the total frequency should be quantified according to the crystal properties. This allows writing the total frequency as follows [19, 33, 34]:

$$\Delta f = F_i - F_0 = \Delta f_m + \Delta f_T + \Delta f_p + \Delta f_r + \Delta f_{\eta,\rho}, \tag{4}$$

with, Δf_m being the effect of the mass variation, Δf_T being the effect of the temperature variation, Δf_p being the effect of the pressure variation, Δf_r being the effect of the crystal roughness, and $\Delta f_{\eta,\rho}$ being the influences of the liquid properties (viscosity and density of the solution) described by Kanazawa and Gordon [33].

Indeed, the influences of the temperature and the roughness on the total frequency should be neglected since the present investigation was carried out using polished crystals at a fixed temperature. The hydrostatic pressure influence was not taken into account according to Equation (2). Furthermore, low effects of the solution properties were noted, so they were not considered. Thus, the impact of the variation of the deposited mass is the dominant factor for the frequency change ($\Delta f = \Delta f_m$). This means that the experimental measurements of the frequency variations characterize only the interactions between the metals and the adsorbent sites of porphyrins. Therefore, the physicochemical characterization of the adsorption process should be only focus on the analysis of the interactions between the ions and the porphyrins without taking account of the quartz crystal sensor because the adsorption process is performed without the intervention of the crystal properties.

In fact, the adsorbed masses Δm (also noted Q_A) of the three adsorbates on the surface after each injection was determined from the resonant frequency variation (Equation (3)).

2.4. Results of Experimental Measurements. The experimental adsorbed quantities of Al^{3+}, Fe^{3+}, and In^{3+} on H_2TPP and H_2TTPP are plotted in Figure 4 at 290-330 K.

Observing carefully the experimental data of the six adsorption systems, it is clear that the behavior of the isotherm curve depends on the type of adsorbate. The isotherms of aluminum chloride on H_2TTPP and H_2TPP (systems (a) and (a′)) show the same behavior (a unique saturation level for all the temperatures). This indicates that the two porphyrin supports adsorbed one layer of aluminum ions without contribution of the chloride ions in the adsorption process. The adsorbed quantities of $FeCl_3$ (systems (b) and (b′)) decrease after the saturation level. In this case, the presence of an irreversible phenomenon is possible at a high iron chloride concentration which reflects weak iron-porphyrin binding. The indium chloride isotherms (systems (c) and (c′)) present two stability states (multilayer ionic adsorption). In this situation, it can be suggested that the two tested porphyrins H_2TPP and H_2TTPP adsorb many layers based on charge neutralization between particles having opposite charge signs (layer-by-layer (LBL) process) [24, 25, 35, 36].

In addition, comparing the performance of the six adsorption systems in terms of quantity, we can note the following order of adsorption performance: Q_A (system (a)) > Q_A (system (a′)) > Q_A (system (b)) > Q_A (system (b′)) > Q_A (system (c)) > Q_A (system (c′)). The adsorbed quantities are the highest for $AlCl_3$-H_2TTPP. Then, the adsorption compounds aluminum chloride and porphyrin H_2TTPP can be recommended for a real application of the metalloporphyrin complex. In the following section, the microscopic investigation of this experimental result is carried out through the physical modeling of the experimental isotherms.

3. Theory/Calculation

3.1. Statistical Physics Theory. The estimated values of the physical model parameters represent the key to understand the adsorption mechanism. The progress of this physical treatment is firstly seen against the well-known model of Langmuir (empirical model) [22]. The Langmuir model is developed by considering that one particle can interact with only one adsorbent site without taking account of the external factors. In general, this assumption led to wrong scientific conclusions. On the contrary, our statistical physics models correct this assumption by introducing a parameter defined by the number of adsorbed particles per adsorption site; it is noted in general by "*n*." This correction can simply provide useful interpretations regarding the adsorption mechanism.

Based on the adsorption isotherm profiles, our statistical physics models can suggest various energies which are linked to different functional groups of the adsorbent surface contrary to the traditional equations of Langmuir [22] or Freundlich [23]. In the same direction, the statistical physics models are able to estimate the total number of the formed layer at all the reaction temperatures [24–26]. Note also that the multilayer adsorption of charged ions can be only carried out via a layer-by-layer (LBL) process [25, 36].

A general analysis of the adsorption data led to test two models: the monolayer model for $AlCl_3$ and $FeCl_3$ and the LBL multilayer model for $InCl_3$. The modeling work is then arranged as follows: (a) it is worth mentioning the general methodology which allows developing the physical models

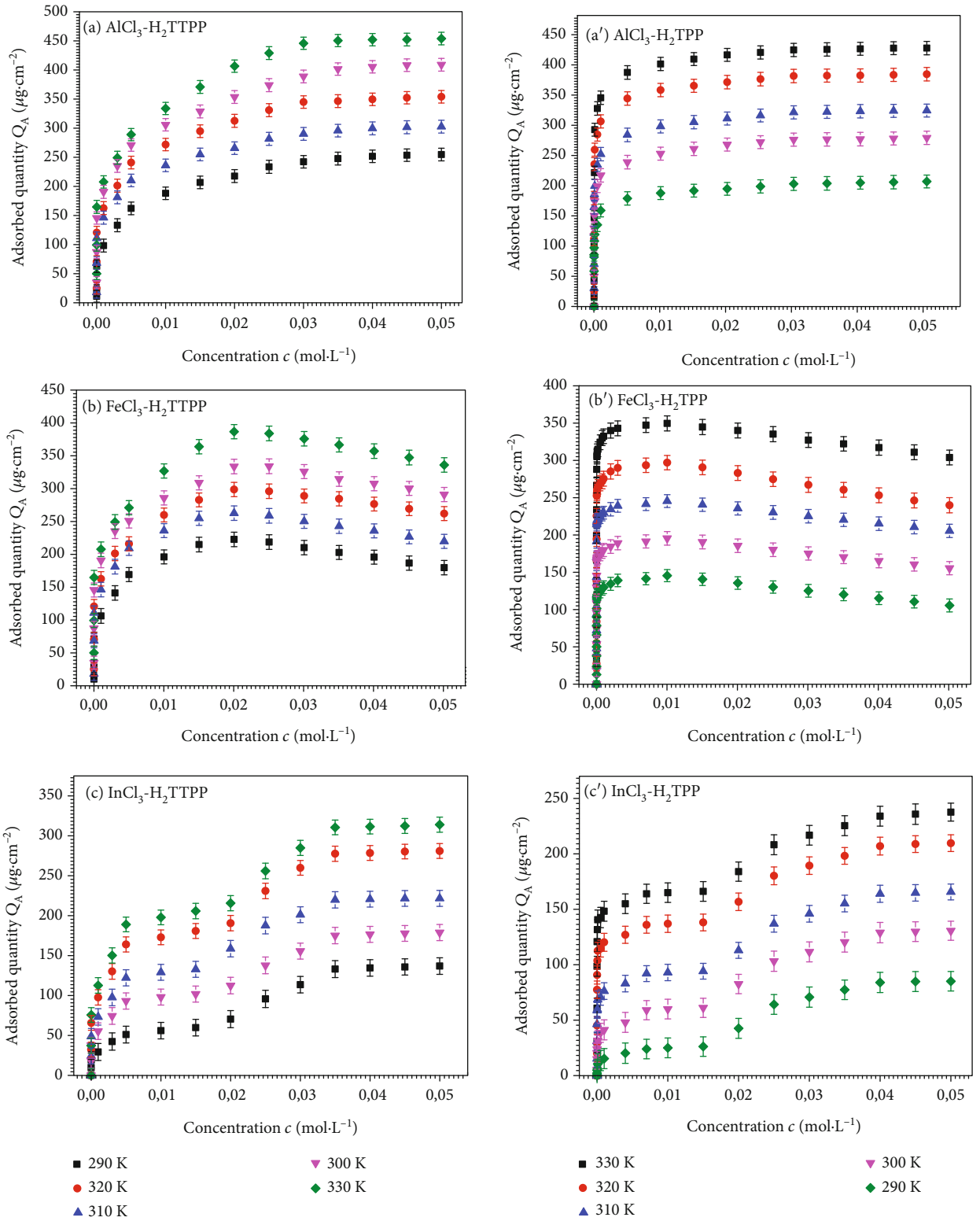

Figure 4: Experimental isotherms of the six adsorption systems given at five temperatures (290-330 K): system (a) $AlCl_3$-H_2TTPP, system (a′) $AlCl_3$-H_2TPP, system (b) $FeCl_3$-H_2TTPP, system (b′) $FeCl_3$-H_2TPP, system (c) $InCl_3$-H_2TTPP, and system (c′) $InCl_3$-H_2TPP.

expressing the adsorbed amount corresponding to the adsorbate concentration, (b) the statistical physics model can be applied and discussed on the experimental data, and (c) the choice of the adopted model led to describing the adsorption reaction via its parameters.

3.2. Advanced Adsorption Models. To establish the physical model expressions, the equilibrium of the adsorption reaction can be expressed via the next equation [25, 37]:

$$nA + S \rightleftarrows A_n - S, \tag{5}$$

where A represents the tested adsorbates ($AlCl_3$/$FeCl_3$/$InCl_3$), S is the adsorbent receptor site of porphyrin (H_2TPP or H_2TTPP), and $A_n - S$ is the resulting complex. The variable n is a stoichiometric parameter which describes the number of bonded ions per adsorbent site. In general, this parameter can identify the nature of the adsorption process ($n \leq 1$: multi-interaction process, $n \geq 1$: multi-ionic process) [38, 39].

This system is characterized by the chemical potential (μ) and the temperature (T) imposing from the outside towards the considered system (grand canonical situation). In this case, the general expression of the partition function is written as a function of the occupation number (N_i), the adsorption energy ($-E_i$), and the Boltzmann factor (β) [37]:

$$z_{gc} = \sum_{N_i} e^{-\beta(-E_i-\mu)N_i}. \tag{6}$$

Concerning the adsorption via one energy level ($-E$) (one adsorbed layer), it can be expressed by [39]

$$z_{gc} = 1 + e^{\beta(E+\mu)}. \tag{7}$$

For the LBL adsorption process (double-layer or multilayer), two energies can be responsible for this process. Note that the adsorption of the first layer is characterized by the energy ($-E_1$), and the second energy ($-E_2$) is in relationship with the formation of the additional adsorbed layers. The partition function is written as [38] follows:

For the double-layer model:

$$z_{gc} = 1 + e^{\beta(E_1+\mu)} + e^{\beta(E_1+E_2+2\mu)}. \tag{8}$$

For the multilayer model:

$$z_{gc} = 1 + e^{\beta(E_1+\mu)} + \sum_{N_i=2}^{L} e^{-\beta(-E_1-(N_i-1)E_2-N_i\mu)}, \tag{9}$$

with L as the number of adsorbed layers.

Then, the average occupation number of P_M porphyrin sites for the three models should be calculated using the next equation [37, 40]:

$$N_o = \frac{P_M}{\beta} \frac{\partial \ln\left(z_{gc}\right)}{\partial \mu}. \tag{10}$$

In this modeling work, the analytical development can be carried out by introducing the chemical potential of the perfect gas (μ_p). μ_p is introduced in the mathematical development of the models through its expression which is written as a function of the partition-function of translation (z_{Tr}) and the number of adsorbates (N) [40, 41]:

$$\mu_p = \frac{1}{\beta} \ln\left(\frac{N}{z_{\mathrm{Tr}}}\right), \tag{11}$$

where z_{tr} can be written as a function of Planck's constant, the volume V, and the mass m of the adsorbed particle [37]:

$$z_{\mathrm{Tr}} = V\left(\frac{2\pi m k_B T}{h^2}\right)^{3/2}. \tag{12}$$

The investigation of the adsorption problem can be also performed using the chemical potential (μ_r) of the real gas. In this case, the lateral interactions involving the adsorbates at free state are taken into account by means of the parameters a (the pressure of cohesion) and b (the covolume) [24, 25]:

$$\mu_r = \mu_p + \frac{1}{\beta} \ln \frac{1}{1-bc} + \frac{1}{\beta}\frac{bc}{1-bc} - 2ac. \tag{13}$$

Then, the adsorbed quantity Q_A (μg/cm^2) can be determined by the following equation [37, 40]:

$$Q_A = n \times N_0. \tag{14}$$

Finally, we get the analytical expressions of the six adsorption models:

The monolayer model of the ideal gas approach:

$$Q_A = nP_M \times \left(\frac{(c/c_{1/2})^n}{1 + (c/c_{1/2})^n}\right), \tag{15}$$

where $c_{1/2}$ involves the molar adsorption energy ($-\Delta E_{1/2}$) (kJ/mol), the adsorption temperature T (K), and the adsorbate solubility S (mol/L). It has the following formula:

$$c_{1/2} = Se^{-(\Delta E_{1/2}/RT)}. \tag{16}$$

The monolayer model of the real gas approach:

$$Q_A = \frac{nP_M}{1 + \left(w_{1/2}((1-bc)/c)e^{2\beta ac}e^{-(bc/(1-bc))}\right)^n}, \tag{17}$$

where the energetic coefficient $w_{1/2}$ is

$$w_{1/2} = Se^{-(\Delta E_{1/2}/RT)}. \tag{18}$$

The double-layer and multilayer models include two energetic coefficients involving two molar adsorption energies ($-\Delta E_1$) and ($-\Delta E_2$).

Table 1: Values of the error adjustment coefficients R^2, RMSE, and AIC deduced from fitting the experimental isotherms of $AlCl_3$, $FeCl_3$, and $InCl_3$ on 5,10,15,20-tetrakis(4-methylphenyl) porphyrin H_2TTPP (systems (a), (b), and (c)) with the three advanced models.

Adsorption model	Monolayer model (ideal gas)			Monolayer model (real gas)			Double-layer model (ideal gas)		
Adjustment coefficient	R^2	RMSE	AIC	R^2	RMSE	AIC	R^2	RMSE	AIC
Adsorption system (a): $AlCl_3$-H_2TTPP									
290 K	0.98	1.23	14.99	0.93	2.64	19.88	0.90	2.98	22.99
300 K	0.99	1.22	15.02	0.94	2.88	19.84	0.91	2.99	23.64
310 K	0.98	1.56	18.71	0.95	2.97	20.34	0.92	2.93	23.84
320 K	0.99	1.34	17.64	0.93	2.56	19.65	0.89	3.01	21.98
330 K	0.98	1.89	16.76	0.94	3.24	20.89	0.91	4.02	22.76
Adsorption system (b): $FeCl_3$-H_2TTPP									
290 K	0.83	5.02	29.01	0.98	1.13	20.51	0.92	2.81	24.72
300 K	0.84	5.12	28.91	0.98	1.11	20.3	0.91	2.98	24.61
310 K	0.82	5.49	28.23	0.99	1.23	21.44	0.93	3.07	25.94
320 K	0.82	4.99	28.99	0.97	1.32	20.98	0.91	3.51	25.16
330 K	0.82	5.01	28.54	0.97	1.29	21.52	0.92	3.11	25.28
Adsorption system (c): $InCl_3$-H_2TTPP									
290 K	0.62	7.89	36.66	0.89	5.77	30.76	0.98	1.98	27.02
300 K	0.71	7.92	36.7	0.88	5.64	30.72	0.99	2.11	27.64
310 K	0.65	8.13	39.4	0.87	6.78	32.65	0.99	1.99	26.91
320 K	0.64	8.13	38.8	0.82	6.36	31.47	0.97	1.98	26.98
330 K	0.67	7.62	38.4	0.79	5.73	32.28	0.97	2.02	26.56

Table 2: Values of the error fitting coefficients R^2, RMSE, and AIC deduced from the numerical adjustment of experimental data of $AlCl_3$, $FeCl_3$, and $InCl_3$ on tetraphenylporphyrin H_2TPP (systems (a′), (b′), and (c′)) with the three statistical physics models.

Adsorption model	Mono-layer model (ideal gas)			Mono-layer model (real gas)			Double-layer model (ideal gas)		
Adjustment coefficient	R^2	RMSE	AIC	R^2	RMSE	AIC	R^2	RMSE	AIC
Adsorption system (a′): $AlCl_3$-H_2TPP									
290 K	0.98	1.11	11.89	0.92	3.44	15.67	0.89	3.89	18.22
300 K	0.97	1.12	12.33	0.93	3.12	15.80	0.90	3.83	18.51
310 K	0.98	1.32	13.56	0.93	3.17	16.42	0.89	3.99	19.56
320 K	0.99	1.36	13.64	0.94	3.43	17.02	0.89	4.15	19.20
330 K	0.98	1.59	14.52	0.93	3.51	16.45	0.92	4.17	18.92
Adsorption system (b′): $FeCl_3$-H_2TPP									
290 K	0.81	4.02	22.31	0.98	1.89	14.30	0.90	3.24	18.22
300 K	0.85	4.54	23.52	0.97	1.82	14.76	0.92	3.54	18.97
310 K	0.83	4.72	23.54	0.98	1.73	15.64	0.94	3.61	19.45
320 K	0.84	4.99	22.92	0.96	1.71	15.99	0.92	4.04	18.83
330 K	0.83	5.15	23.64	0.98	1.66	15.78	0.91	4.22	19.34
Adsorption system (c′): $InCl_3$-H_2TPP									
290 K	0.73	6.66	30.14	0.86	4.54	26.12	0.97	1.28	19.04
300 K	0.73	6.51	31.24	0.85	4.82	26.45	0.98	1.34	20.42
310 K	0.75	7.21	30.74	0.83	4.71	27.08	0.99	1.52	20.84
320 K	0.74	7.54	31.67	0.80	5.02	27.64	0.98	1.49	20.94
330 K	0.71	6.94	31.84	0.82	5.64	27.54	0.98	1.69	21.06

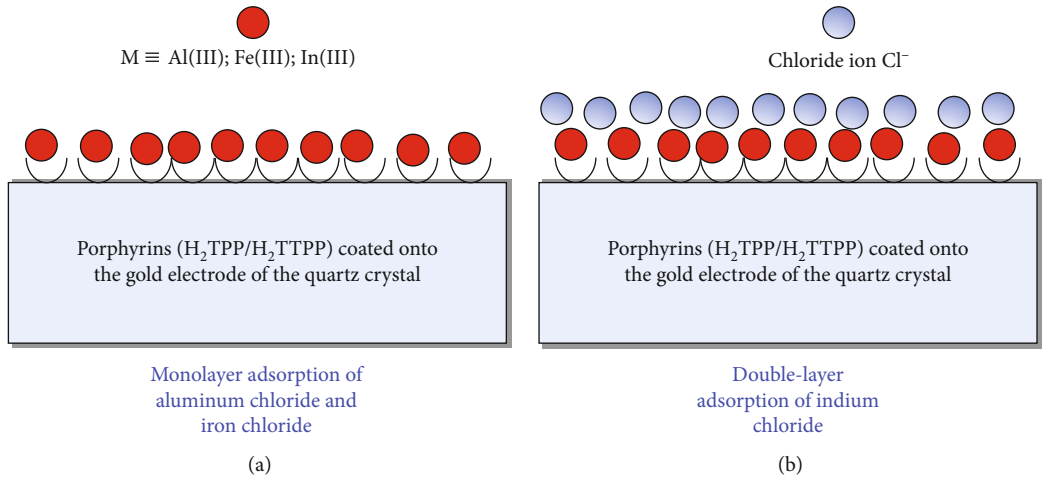

FIGURE 5: Illustration of the monolayer adsorption of $AlCl_3$ and $FeCl_3$ and the LBL double-layer adsorption of $InCl_3$ on the two porphyrins H_2TPP and H_2TTPP.

The double-layer model of the ideal gas approach:

$$Q_A = nP_M \frac{(c/c_1)^n + 2(c/c_2)^{2n}}{1 + (c/c_1)^n + (c/c_2)^{2n}}, \tag{19}$$

where the energetic variables c_1 and c_2 are

$$c_{1,2} = Se^{-(\Delta E_{1,2}/RT)}. \tag{20}$$

The double-layer model of the real gas approach:

$$Q_A = nP_M \frac{\left(c/w_1(1-bc)e^{2\beta ac}e^{-(bc/(1-bc))}\right)^n + 2\left(c/w_2(1-bc)e^{2\beta ac}e^{-(bc/(1-bc))}\right)^{2n}}{1 + \left(c/w_1(1-bc)e^{2\beta ac}e^{-(bc/(1-bc))}\right)^n + \left(c/w_2(1-bc)e^{2\beta ac}e^{-(bc/(1-bc))}\right)^{2n}}, \tag{21}$$

where w_1 and w_2 are

$$w_{1,2} = Se^{-(\Delta E_{1,2}/RT)}. \tag{22}$$

The multilayer model of the ideal gas approach:

$$Q_A = nP_M \times \left(\frac{(c/c_1)^n + (c/c_1)^n(c/c_2)^n\left(1 - 2(c/c_2)^{nL} - L(c/c_2)^{n(L+1)} + (c/c_2)^n\left(1 - (c/c_2)^{nL}\right)/\left(1 - (c/c_2)^n\right)\right)}{(1 - (c/c_1)^n)(1 - (c/c_2)^n) + (c/c_1)^n(c/c_2)^n\left(1 - (c/c_2)^{nL}\right)}\right), \tag{23}$$

where c_1 and c_2 are given by Equation (20).
The multilayer model of the real gas approach:

$$Q_A = nP_M \times \left(\frac{(c/c_1)^n + (c/c_1)^n(c/c_2)^n\left(1 - 2(c/c_2)^{nL} - L(c/c_2)^{n(L+1)} + (c/c_2)^n\left(1 - (c/c_2)^{nL}\right)/\left(1 - (c/c_2)^n\right)\right)}{(1 - (c/c_1)^n)(1 - (c/c_2)^n) + (c/c_1)^n(c/c_2)^n\left(1 - (c/c_2)^{nL}\right)}\right), \tag{24}$$

where c_1 and c_2 are written as

$$c_{1,2} = w_{1,2}(1 - bc)e^{2\beta ac}e^{-(bc/(1-bc))}, \tag{25}$$

with w_1 and w_2 are previously mentioned (Equation (22)).

3.3. Adjustment of Adsorption Models with Experimental Isotherms. The six physical adsorption models were applied on the experimental isotherms by means of a numerical fitting program [42]. The mathematical fitting method is based on the Levenberg-Marquardt iterating algorithm using a multivariable nonlinear regression program [40, 43]. The criteria to adopt a descriptive model are the determination coefficient R^2, the RMSE coefficient (residual root mean square error), and the well-known AIC (Akaike Information Criterion) coefficient. The first error coefficient (R^2) is a standardized measure of the fit goodness [43, 44]. If the coefficient R^2 value is near the unit, we are in the case of the best fitting model. The second error coefficient (RMSE) is a nonstandardized measure of the fit goodness [44–47]. The best fitting model is obtained when the RMSE value is inferior to 2. The third adjustment coefficient (AIC) shows the best fitting with the model having the lowest AIC values [36]. These three adjustment coefficients are interpreted to adopt a physical model.

Tables 1 and 2 show the numerical values of the error adjustment coefficients.

According to Tables 1 and 2, the aluminum chloride isotherms (systems (a) and (a′)) should be analyzed by the monolayer model of ideal gas which shows R^2 values near the unit and low values of RMSE and AIC for the five reaction temperatures. However, the adsorption isotherms of $FeCl_3$ (systems (b) and (b′)) show the best coefficients of adjustment with the monolayer model of real gas. This explains that the decline of the $FeCl_3$ isotherms at high equilibrium concentration is fundamentally due to the lateral interaction impacts and confirms that the

Table 3: Values of the physicochemical parameters (n, P_M, a, b, $c_{1/2}$, $w_{1/2}$, c_1, and c_2) affecting the adsorption of $AlCl_3$, $FeCl_3$, and $InCl_3$ on 5,10,15,20-tetrakis(4-methylphenyl) porphyrin H_2TTPP (systems (a), (b), and (c)) at five temperatures.

System	Parameters	290 K	300 K	310 K	320 K	330 K
System (a): $AlCl_3$-H_2TTPP	n	0.80 (±0.02)	0.81 (±0.015)	0.89 (±0.019)	0.99 (±0.024)	1.01 (±0.019)
	P_m	281.7 (±8.2)	320.6 (±9.4)	366.1 (±8.9)	401.9 (±10.9)	450.7 (±11.7)
	$c_{1/2}$	0.015 (±0.005)	0.015 (±0.006)	0.016 (±0.005)	0.016 (±0.005)	0.017 (±0.006)
System (b): $FeCl_3$-H_2TTPP	n	0.71 (±0.025)	0.73 (±0.015)	0.79 (±0.022)	0.84 (±0.019)	0.89 (±0.02)
	P_m	228.4 (±12.1)	262.6 (±10.9)	298.7 (±9.99)	333.6 (±8.79)	389.8 (±9.78)
	$w_{1/2}$	0.011 (±0.004)	0.011 (±0.005)	0.012 (±0.006)	0.011 (±0.006)	0.012 (±0.007)
	a ($\times 10^{-9}$)	8.3 (±0.2)	7.2 (±0.3)	6.1 (±0.4)	5.8 (±0.3)	5.1 (±0.5)
	b ($\times 10^{-12}$)	2.6 (±0.1)	3.2 (±0.2)	3.9 (±0.2)	4.8 (±0.4)	5.7 (±0.4)
System (c): $InCl_3$-H_2TTPP	n	0.63 (±0.018)	0.66 (±0.023)	0.69 (±0.016)	0.74 (±0.022)	0.82 (±0.016)
	P_m	142.3 (±9.52)	189.4 (±10.7)	233.8 (±12.8)	289.4 (±11.2)	320.5 (±10.9)
	c_1	0.0033 (±0.0007)	0.003 (±0.008)	0.0035 (±0.0003)	0.0032 (±0.0009)	0.0036 (±0.0004)
	c_2	0.026 (±0.007)	0.025 (±0.009)	0.026 (±0.008)	0.025 (±0.004)	0.027 (±0.007)

Table 4: Values of the physicochemical variables (n, P_M, a, b, $c_{1/2}$, $w_{1/2}$, c_1, and c_2) deduced from the fitting of experimental data of $AlCl_3$, $FeCl_3$, and $InCl_3$ on tetraphenylporphyrin H_2TPP (systems (a′), (b′), and (c′)) with the three adopted models.

System	Parameters	290 K	300 K	310 K	320 K	330 K
System (a′): $AlCl_3$-H_2TPP	n	0.75 (±0.021)	0.77 (±0.026)	0.83 (±0.019)	0.91 (±0.023)	0.95 (±0.017)
	P_m	258.2 (±12.2)	301.2 (±9.77)	332.7 (±8.97)	368.2 (±9.65)	421.4 (±10.7)
	$c_{1/2}$	0.009 (±0.0007)	0.011 (±0.006)	0.009 (±0.0008)	0.01 (±0.003)	0.008 (±0.0009)
System (b′): $FeCl_3$-H_2TPP	n	0.67 (±0.023)	0.70 (±0.019)	0.74 (±0.02)	0.79 (±0.022)	0.85 (±0.016)
	P_m	184.5 (±9.71)	231.4 (±8.69)	268.2 (±9.43)	312.2 (±10.3)	355.2 (±8.46)
	$w_{1/2}$	0.007 (±0.0002)	0.008 (±0.0001)	0.008 (±0.0003)	0.0075 (±0.0001)	0.0069 (±0.0006)
	a ($\times 10^{-9}$)	10.5 (±0.8)	9.4 (±0.9)	8.4 (±0.6)	7.9 (±0.5)	7.12 (±0.5)
	b ($\times 10^{-12}$)	1.2 (±0.2)	1.7 (±0.1)	2.4 (±0.1)	3.3 (±0.2)	4.1 (±0.3)
System (c′): $InCl_3$-H_2TPP	n	0.50 (±0.015)	0.56 (±0.016)	0.61 (±0.015)	0.70 (±0.019)	0.79 (±0.02)
	P_m	105.4 (±7.89)	147.3 (±8.45)	194.3 (±10.5)	238.4 (±9.34)	279.4 (±8.64)
	c_1	0.002 (±0.0007)	0.003 (±0.006)	0.0031 (±0.0009)	0.0029 (±0.008)	0.0032 (±0.0005)
	c_2	0.023 (±0.005)	0.024 (±0.007)	0.025 (±0.003)	0.025 (±0.008)	0.026 (±0.002)

aluminum ions are the best compounds for porphyrin complexation in terms of stability. On the other hand, in light of the selection criteria, the indium chloride adsorption (systems (c) and (c′)) should be described via the double-layer model of ideal gas. In this case, two adsorbed layers are formed based on charge neutralization between cations (In^{3+}) and anions (Cl^-).

Figure 5 illustrates the monolayer adsorptions of aluminum chloride and iron chloride and the double-layer adsorption of indium chloride on H_2TTP and H_2TPP.

3.4. Analysis of Physicochemical Parameters. The mon-layer model (ideal gas), devoted for the description of the $AlCl_3$ isotherms, was governed by three parameters (the number of aluminum ions per receptor site n, the number of porphyrin sites P_M, and the energetic parameter $c_{1/2}$ (Equation (16))). For $FeCl_3$, the monolayer model (real gas) presents the parameter a (cohesion pressure) and the parameter b (covolume) in addition to the steric variables n and P_m and the energetic parameter $w_{1/2}$. The LBL double-layer adsorption of $InCl_3$ can be interpreted via four physicochemical variables (n and P_M (steric variables) and c_1 and c_2 (Equation (20))).

All fitting parameters values are given in Tables 3 and 4. The study of the adsorption model parameters attributes interesting microscopic interpretations of the porphyrin complexation.

3.4.1. Steric Interpretation. Basically, the parameters n and P_M are typified by a steric aspect. The product of these parameters is the result of the maximum adsorption capacity [48].

The evolution of the two steric parameters versus temperature is reported in Figure 6.

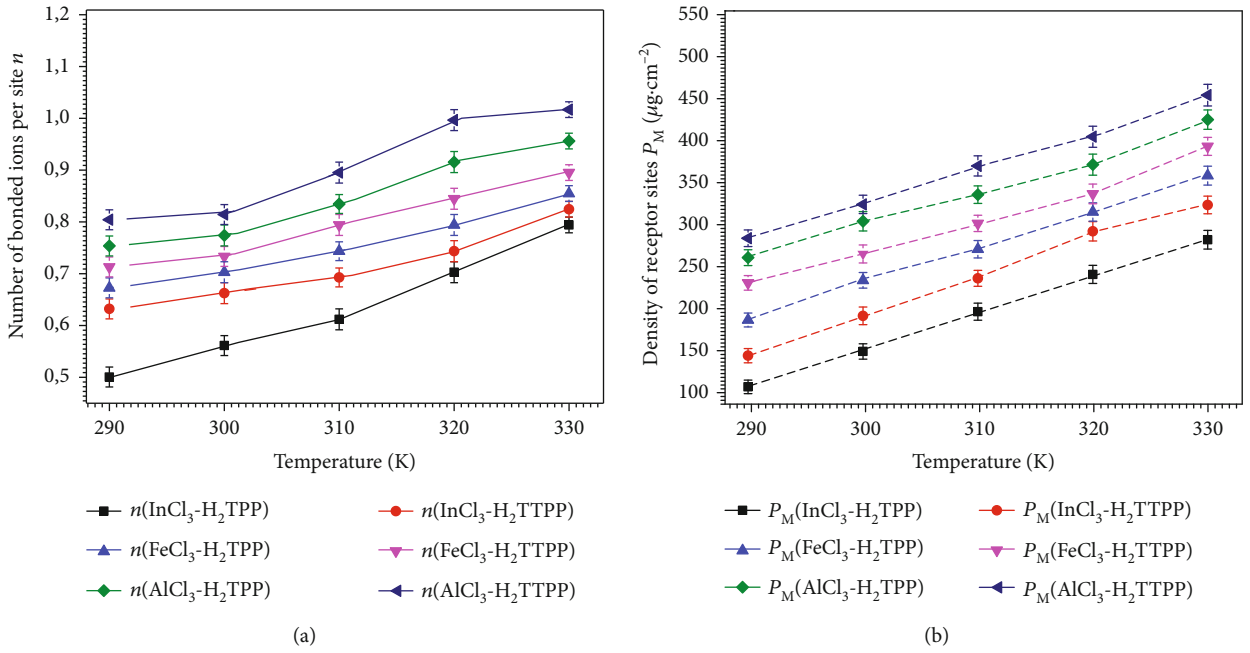

FIGURE 6: Evolutions of the two steric parameters as a function of temperature: (a) evolution of the number of bonded ions per site n and (b) variation of the density of receptor porphyrin sites P_M.

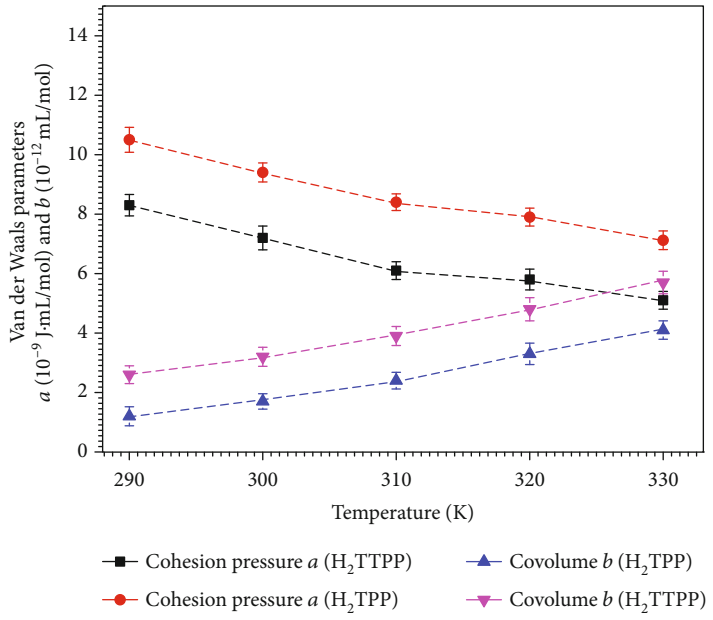

FIGURE 7: Variations of the adjusted values of the cohesion pressure a and the covolume b as a function of temperature (290-330 K) for the indium chloride adsorption.

From Figure 6(a), the n values are found inferior to 1 for the six adsorption systems. For example, regarding the values of this parameter that are inferior to 0.5, it is clear that the complexation mechanism is a multi-interaction process (the ions can be interacted with two adsorption sites) [39].

The fitted values of P_M describe the number of porphyrin sites accessible to the adsorbate ions at each temperature. Figure 6(b) demonstrates that the adsorptions of $AlCl_3$ and $FeCl_3$ present the highest values of P_M at all the temperatures: P_M ($AlCl_3$) > P_M ($FeCl_3$) > P_M ($InCl_3$). In fact, the anions are not involved in the complexation processes of $AlCl_3$ and $FeCl_3$, so there is a fast insertion of the metallic ions in the porphyrin cavities. However, the contribution of the anionic particles in $InCl_3$ adsorption prevents the complexation of porphyrin by the indium ions because of the interaction between the two adsorbed layers.

Furthermore, it is noted from Figure 4 that the temperature exerts exactly the same influence on the six

Table 5: Values of the molar adsorption energies $|-\Delta E_{1/2}|$ for $AlCl_3$ and $FeCl_3$ adsorptions and $|-\Delta E_1|$ and $|-\Delta E_2|$ for $InCl_3$ adsorption given in modulus values at 290, 300, 310, 320, and 330 K.

Adsorption system	Adsorption energy	290 K	300 K	310 K	320 K	330 K
System (a): $AlCl_3$-H_2TTPP	$\lvert-\Delta E_{1/2}\rvert$ (kJ/mol)	61.4 (±2.1)	69.5 (±2.3)	70.6 (±3.1)	75.4 (±2.9)	80.3 (±3.9)
System (a′): $AlCl_3$-H_2TPP	$\lvert-\Delta E_{1/2}\rvert$ (kJ/mol)	48.4 (±2.1)	57.2 (±2.4)	60.2 (±1.8)	63.4 (±3.1)	67.4 (±2.9)
System (b): $FeCl_3$-H_2TTPP	$\lvert-\Delta E_{1/2}\rvert$ (kJ/mol)	32.9 (±1.8)	36.4 (±1.7)	38.7 (±2.5)	40.8 (±2.2)	43.1 (±2.3)
System (b′): $FeCl_3$-H_2TPP	$\lvert-\Delta E_{1/2}\rvert$ (kJ/mol)	30.2 (±1.9)	33.6 (±1.8)	36.7 (±1.8)	38.4 (±2.1)	40.9 (±2.2)
System (c): $InCl_3$-H_2TTPP	$\lvert-\Delta E_1\rvert$ (kJ/mol)	26.4 (±2.3)	30.4 (±1.6)	33.5 (±1.5)	36.8 (±1.9)	38.7 (±1.7)
	$\lvert-\Delta E_2\rvert$ (kJ/mol)	17.2 (±1.2)	20.4 (±1.5)	23.3 (±1.4)	25.7 (±1.1)	28.8 (±1.6)
System (c′): $InCl_3$-H_2TPP	$\lvert-\Delta E_1\rvert$ (kJ/mol)	22.3 (±2.7)	26.1 (±2.4)	29.4 (±2.1)	33.1 (±1.9)	35.6 (±1.8)
	$\lvert-\Delta E_2\rvert$ (kJ/mol)	12.7 (±1.5)	16.7 (±1.6)	18.9 (±2.0)	20.4 (±2.1)	21.1 (±1.8)

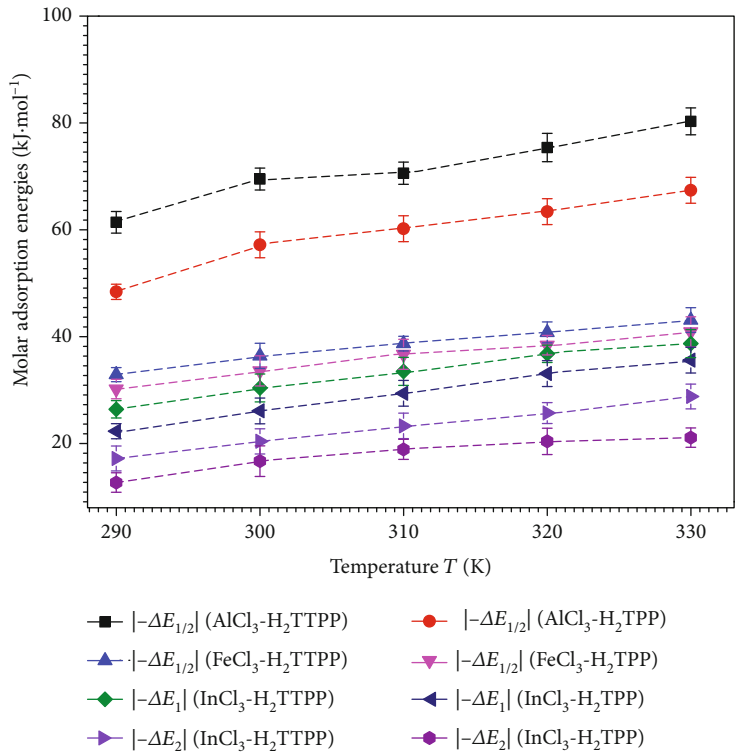

Figure 8: Evolutions of the molar adsorption energies of the six adsorption systems as a function of temperature: $|-\Delta E_{1/2}|$ for $AlCl_3$ and $FeCl_3$, and $|-\Delta E_1|$ and $|-\Delta E_2|$ for $InCl_3$.

complexation systems: once the temperature increases, the adsorption capacities increase. This is often explained from Figure 6 which shows that the values of the coefficients n (Figure 6(a)) and P_M (Figure 6(b)) rise with the temperature. It can be concluded that the thermal agitation effect favors the adsorption dynamics: the rise of temperature activates other receptor sites to contribute in the complexation process.

3.4.2. Van der Waals Parameter Behaviors. It can be noticed that despite the $AlCl_3$ and $FeCl_3$ adsorptions being both monolayer adsorption processes, where there is no contribution of the chloride ions at the layer formation, the fitted values of P_M are the lowest for $FeCl_3$. Thus, the physical model that describes the $FeCl_3$ adsorption includes the lateral interaction effect by the intermediate of the parameter a (cohesion pressure) and the parameter b (covolume) [49].

It can be concluded that the decrease of $FeCl_3$ isotherms (Figures 4(b) and 4(b′)) can be the result of the high adsorbate-adsorbate interaction which reflects a weak binding Fe^{3+}-porphyrin compared to the Al^{3+}-porphyrin binding.

Overall, it can be concluded that the use of aluminum chloride guarantees more stability during the metalloporphyrin formation.

The values of these two parameters for H_2TPP and H_2TTPP are summarized in Figure 7.

Generally, the interactions of the particles (lateral interactions) are characterized by the cohesion pressure a. One can see from Figure 7 that $a(FeCl_3\text{-}H_2TTPP) < a(FeCl_3\text{-}H_2TPP)$. Therefore, the H_2TTPP is the best complexing porphyrin of the iron ions because it presents the lowest impact of the lateral interactions on the adsorption process. On the other hand, it should be noted, from Figure 7, that the H_2TTPP presents the highest values of the covolume b: $b(FeCl_3\text{-}H_2TTPP) > b(FeCl_3\text{-}H_2TPP)$. In this case, the distance between the adsorbates is high which indicates that the iron ions can be easily adsorbed by the surface and causes an expansion in the adsorbed amount. This result confirms the suggestion of the porphyrin H_2TTPP as a suitable material for the metalloporphyrin adsorption.

Furthermore, it is seen from Figure 7 that the parameter a declines with the expansion of the temperature for the FeCl3 adsorption while the covolume b increases. The decrease of the cohesion pressure indicates that the lateral interaction effect is low at high temperature. The increase of the parameter b reflects a strong distance between the adsorbates. The lateral interaction description explains the highest performance of the iron adsorption at 330 K and shows the endothermic nature of the studied process.

3.4.3. Energetic Calculation. According to Equations (16), (18), and (20), the molar energies of the six adsorption mechanisms can be calculated by means of the energetic coefficients, $c_{1/2}$ for $AlCl_3$, $w_{1/2}$ for $FeCl_3$, and c_1 and c_2 for $InCl_3$, which are calculated from the numerical simulation of the three adopted models [36, 48].

For aluminum chloride adsorption,

$$-\Delta E_{1/2} = RT \times \ln\left(\frac{c_{1/2}}{S(AlCl_3)}\right). \quad (26)$$

For iron chloride adsorption,

$$-\Delta E_{1/2} = RT \times \ln\left(\frac{w_{1/2}}{S(FeCl_3)}\right). \quad (27)$$

For indium chloride adsorption,

$$-\Delta E_1 = RT \times \ln\left(\frac{c_1}{S(InCl_3)}\right), \quad (28)$$

$$-\Delta E_2 = RT \times \ln\left(\frac{c_2}{S(InCl_3)}\right). \quad (29)$$

The values of the molar energies and their variations via the temperature are reported in Table 5 and Figure 8.

According to Table 5, for the indium chloride adsorption, it is obviously remarked that the calculated values of $|(-\Delta E_1)|$ which characterizes the indium-porphyrin interaction are greater than those of $|(-\Delta E_2)|$ (interaction between the two adsorbed layers [36]). Therefore, we can conclude that the interaction $|(-\Delta E_1)|$ should be compared to the other adsorption system energies ($|(-\Delta E_{1/2})|$) to evaluate the stability of the formed metalloporphyrin complexes.

Comparing the $|(-\Delta E_{1/2})|$ and the $|(-\Delta E_1)|$ values of the six complexation systems (Table 5 and Figure 8), we observe that $|(-\Delta E_{1/2})|\ (AlCl_3\text{-}H_2TTPP) > |(-\Delta E_{1/2})|\ (AlCl_3\text{-}H_2TPP) > |(-\Delta E_1)|\ (FeCl_3\text{-}H_2TTPP) > |(-\Delta E_1)|\ (FeCl_3\text{-}H_2TPP) > |(-\Delta E_{1/2})|\ (InCl_3\text{-}H_2TTPP) > |(-\Delta E_{1/2})|\ (InCl_3\text{-}H_2TPP)$. It can be noticed that the affinity of the porphyrin H_2TTPP cavities to the metallic ions is higher than the tetraphenylporphyrin sites H_2TPP for the three ions and confirms that the aluminum chloride-porphyrin (H_2TTPP) is the best adsorption system suited for metalloporphyrin application because it presents the highest adsorption energies values for the five reaction temperatures.

It can be also observed that the molar energies rise with the expansion of the temperature (Figure 8). This can be interpreted by the endothermic behavior of the six studied processes.

Furthermore, the energies $|(-\Delta E_{1/2})|$ of $AlCl_3$ are superior to 40 kJ/mol for all the temperatures. For this system, the adsorption is carried out via a chemical process involving covalent bonds (irreversible phenomenon) [39, 50–52]. In this case, the adsorption is a dissociative mechanism (there is no possibility of a desorption process) because there is a change in the electron density between the adsorbent and the adsorbed particle. Moreover, a multilayer adsorption is impossible due to the high interaction between the adsorbed layer and the adsorbent surface (e.g., $AlCl_3$ adsorption).

In contrast, all the other adsorption mechanisms ($FeCl_3$ and $InCl_3$) take place via a physical process since they present adsorption energy values lower than 40 kJ/mol [42, 50, 51]. During physisorption, the adsorbed particles retain their individual properties and there is no change in the structure of the components of the adsorption system. The system is weakly energetic (low adsorbate-adsorbent interaction), so the presence of a desorption phenomenon is possible (e.g., $FeCl_3$ adsorption). Moreover, the adsorbed layer can interact with other adsorbed layers and can act as a new template for the adsorption of the following layer (multilayer adsorption mechanism) such as the case of $InCl_3$ in the present investigation.

4. Conclusion

In this work, the experimental QCM tool is used to control the adsorption of aluminum chloride, iron chloride, and indium chloride on porphyrins H_2TTPP and H_2TPP. By analyzing the experimental isotherms, the $AlCl_3\text{-}H_2TTPP$ complex was found as the best adsorption system in terms of reproducibility since it showed the highest adsorbed quantities. Theoretically, statistical physical models were suggested for the analysis of the experimental results. The numerical investigation confirmed that the chloride ions contributed only in the adsorption of $InCl_3$ (double-layer adsorption). The iron chloride adsorption was described by a monolayer model that considers the lateral interactions of the ions indicating the lowest stability of the formed iron-porphyrin complex. The physicochemical parameters of these models gave interesting microscopic insights about the complexation of the two porphyrins. Indeed, it was found that the six adsorption processes were governed by a multi-interaction process

(n is inferior to 1). The thermal agitation caused an increase of the number of occupied sites P_M which indicated that some porphyrin sites contributed to the adsorption only at high temperature (endothermic process). The energetic study, through adsorption energy calculation, demonstrated that the adsorption of $AlCl_3$ on H_2TTPP is a chemisorption process involving covalent bonds.

Data Availability

The data that supports the findings of this study are available within the article.

Conflicts of Interest

The authors declare that they have no conflicts of interest.

Acknowledgments

The authors extend their appreciation to the Deputyship for Research & Innovation, Ministry of Education – Kingdom of Saudi Arabia for funding this research through project number PNU-DRI-RI-20-016.

References

[1] J. Fuchs, S. Weber, and R. Kaufmann, "Genotoxic potential of porphyrin type photosensitizers with particular emphasis on 5-aminolevulinic acid: implications for clinical photodynamic therapy," *Free Radical Biology & Medicine.*, vol. 28, no. 4, pp. 537–548, 2000.

[2] G. Simonneaux, H. Srour, P. Le Maux, S. Chevance, and D. Carrie, "Metalloporphyrin symmetry in chiral recognition and enantioselective catalysis," *Symmetry*, vol. 6, no. 2, pp. 210–221, 2014.

[3] B. Saha, A. G. Petrovic, A. Dhamija, N. Berova, and S. P. Rath, "Complexation of chiral zinc(II) porphyrin tweezer with achiral aliphatic diamines revisited: molecular dynamics, electronic CD, and ^{1}H NMR analysis," *Inorganic Chemistry*, vol. 58, no. 17, pp. 11420–11438, 2019.

[4] J. Du, C. Miao, C. Xia, Y. M. Lee, W. Nam, and W. San, "Mechanistic insights into the enantioselective epoxidation of olefins by bioinspired manganese complexes: role of carboxylic acid and nature of active oxidant," *ACS Catalysis*, vol. 8, no. 5, pp. 4528–4538, 2018.

[5] K. M. Mullen and M. J. Gunter, "Toward Multistation Rotaxanes Using Metalloporphyrin Coordination Templating," *The Journal of Organic Chemistry*, vol. 73, no. 9, pp. 3336–3350, 2008.

[6] M. Guo, T. Corona, K. Ray, and W. Nam, "Heme and nonheme high-valent iron and manganese oxo cores in biological and abiological oxidation reactions," *ACS Central Science*, vol. 5, no. 1, pp. 13–28, 2019.

[7] N. Chaudhri, L. Cong, A. S. Bulbul et al., "Structural, photophysical, and electrochemical properties of doubly fused porphyrins and related fused chlorins," *Inorganic Chemistry*, vol. 59, no. 2, pp. 1481–1495, 2020.

[8] M. S. Liao and S. Scheiner, "Electronic structure and bonding in metal porphyrins, metal=Fe, Co, Ni, Cu, Zn," *The Journal of Chemical Physics*, vol. 117, no. 1, pp. 205–219, 2002.

[9] I. H. A. Badr and M. E. Meyerhoff, "Highly selective optical fluoride ion sensor with submicromolar detection limit based on aluminum(III) octaethylporphyrin in thin polymeric film," *Journal of the American Chemical Society*, vol. 127, no. 15, pp. 5318-5319, 2005.

[10] L. Li, Y. Zhang, Y. Li et al., "Polymeric membrane fluoride-selective electrodes using Lewis acidic organo-antimony(V) compounds as ionophores," *ACS Sensors*, vol. 5, no. 11, pp. 3465–3473, 2020.

[11] P. P. Kumar and B. G. Maiya, "Aluminium(III) porphyrin based dimers and trimers: synthesis, spectroscopy and photochemistry," *New Journal of Chemistry*, vol. 27, no. 3, pp. 619–625, 2003.

[12] Y. Qin, H. Guo, X. Sheng, X. Wang, and F. Wang, "An aluminum porphyrin complex with high activity and selectivity for cyclic carbonate synthesis," *Green Chemistry*, vol. 17, no. 5, pp. 2853–2858, 2015.

[13] I. Ojima, *Catalytic Asymmetric Synthesis*, Wiley-VCH, New York, NY, USA, 2000.

[14] E. Stulz, S. M. Scott, Y. F. Ng et al., "Construction of multiporphyrin arrays using ruthenium and rhodium coordination to phosphines," *Inorganic Chemistry*, vol. 42, no. 20, pp. 6564–6574, 2003.

[15] S. Richeter, J. Thion, A. van der Lee, and D. Leclercq, "Synthesis, structural characterization and properties of aluminum (III) meso-tetraphenylporphyrin complexes axially bonded to phosphinate anions," *Inorganic Chemistry*, vol. 45, pp. 10049–10051, 2006.

[16] X. Liu, H. Pang, X. Liu et al., "Orderly porous covalent organic frameworks-based materials: superior adsorbents for pollutants removal from aqueous solutions," *The Innovation*, vol. 2, no. 1, article 100076, 2021.

[17] N. S. Alharbi, B. Hu, T. Hayat et al., "Efficient elimination of environmental pollutants through sorption-reduction and photocatalytic degradation using nanomaterials," *Frontiers of Chemical Science and Engineering*, vol. 14, no. 6, pp. 1124–1135, 2020.

[18] H. G. Hong and T. E. Mallouk, "Electrochemical measurements of electron transfer rates through zirconium 1,2-ethanediylbis(phosphonate) multilayer films on gold electrodes," *Langmuir*, vol. 7, no. 10, pp. 2362–2369, 1991.

[19] S. H. Cho, S. T. Nguyen, and J. T. Hupp, "Manganese porphyrin multilayer films assembled on ITO electrodes via zirconium phosphonate chemistry: chemical and electrochemical catalytic oxidation activity," *Topics in Catalysis*, vol. 34, no. 1-4, pp. 101–107, 2005.

[20] G. de Ruiter, M. Lahav, and M. E. van der Boom, "Pyridine coordination chemistry for molecular assemblies on surfaces," *Accounts of Chemical Research*, vol. 47, no. 12, pp. 3407–3416, 2014.

[21] D. Wang, P. Mousavi, P. J. Hauser, W. Oxenham, and C. S. Grant, "Quartz crystal microbalance in elevated temperature viscous liquids: temperature effect compensation and lubricant degradation monitoring," *Colloids and Surfaces A: Physicochemical and Engineering Aspects*, vol. 268, no. 1-3, pp. 30–39, 2005.

[22] I. Langmuir, "The adsorption of gases on plane surfaces of glass, mica and platinum," *Journal of the American Chemical Society*, vol. 40, no. 9, pp. 1361–1403, 1918.

[23] F. M. H. Freundlich, "Over the adsorption in solution," *The Journal of Physical Chemistry*, vol. 57, pp. 385–471, 1906.

[24] M. Ben Yahia, M. B. Yahia, F. Aouaini et al., "Adsorption of sodium and lithium ions onto helicenes molecules: experiments and phenomenological modeling," *Journal of Molecular Liquids*, vol. 288, article 110988, 2019.

[25] S. Knani, N. Khalifa, M. Ben Yahia, F. Aouaini, and M. Tounsi, "Statistical physics study of the interaction of the 5, 10, 15, 20-tetrakis (4-tolylphenyl) porphyrin (H_2TTPP) with magnesium ion: new microscopic interpretations," *Arabian Journal of Chemistry*, vol. 13, no. 2, pp. 4374–4385, 2020.

[26] A. Nakbi, M. Bouzid, F. Ayachi, F. Aouaini, and A. B. Lamine, "Investigation of caffeine taste mechanism through a statistical physics modeling of caffeine dose-taste response curve by a biological putative caffeine adsorption process in electrophysiological response," *Progress in Biophysics and Molecular Biology*, vol. 147, pp. 70–85, 2019.

[27] A. D. Adler, F. R. Longo, J. D. Finarelli, J. Goldmacher, J. Assour, and L. Korakoff, "A simplified synthesis for meso-tetraphenylporphine," *The Journal of Organic Chemistry*, vol. 32, no. 2, pp. 476–476, 1967.

[28] P. Buck, E. Lindner, W. Kutner, and G. Inzelt, "Piezoelectric chemical sensors (IUPAC technical report)," *Pure and Applied Chemistry*, vol. 76, no. 6, pp. 1139–1160, 2004.

[29] C. K. O'Sullivan and G. G. Guilbault, "Commercial quartz crystal microbalances theory and applications," *Biosensors and Bioelectronics*, vol. 14, no. 8-9, pp. 663–670, 1999.

[30] G. Sauerbrey, "Verwendung von schwingquarzen zur wägung dünner schichten und zur mikrowägung," *Zeitschrift für Physik*, vol. 155, no. 2, pp. 206–222, 1959.

[31] T. Nomura and M. Okuhara, "Frequency shifts of piezoelectric quartz crystals immersed in organic liquids," *Analytica Chimica Acta*, vol. 142, pp. 281–284, 1982.

[32] V. Tsionsky and E. Gileadi, "Use of the quartz crystal microbalance for the study of adsorption from the gas phase," *Langmuir*, vol. 10, no. 8, pp. 2830–2835, 1994.

[33] K. K. Kanazawa and J. G. Gordon, "Frequency of a quartz microbalance in contact with liquid," *Analytical Chemistry*, vol. 57, no. 8, pp. 1770-1771, 1985.

[34] M. Urbakh and L. Daikhin, "Influence of the surface morphology on the quartz crystal microbalance response in a fluid," *Langmuir*, vol. 10, no. 8, pp. 2836–2841, 1994.

[35] E. Malinowska and M. E. Meyerhoff, "Role of axial ligation on potentiometric response of Co(III) tetraphenylporphyrin-doped polymeric membranes to nitrite ions," *Analytica Chimica Acta*, vol. 300, no. 1-3, pp. 33–43, 1995.

[36] M. Ben Yahia, S. Knani, H. B. L. Hsan, M. B. Yahia, H. Nasri, and A. B. Lamine, "Statistical studies of adsorption isotherms of iron nitrate and iron chloride on a thin layer of porphyrin," *Journal of Molecular Liquids*, vol. 248, pp. 235–245, 2017.

[37] A. Ben Lamine and Y. Bouazra, "Application of statistical thermodynamics to the olfaction mechanism," *Chemical Senses*, vol. 22, no. 1, pp. 67–75, 1997.

[38] S. Knani, M. Mathlouthi, and A. Ben Lamine, "Modeling of the psychophysical response-curves using the grand canonical ensemble in statistical physics," *Food Biophysics*, vol. 2, no. 4, pp. 183–192, 2007.

[39] L. Sellaoui, E. F. Soetaredjo, S. Ismadji et al., "Insights on the statistical physics modeling of the adsorption of Cd^{2+} and Pb^{2+} ions on bentonite-chitosan composite in single and binary systems," *Chemical Engineering Journal*, vol. 354, pp. 569–576, 2018.

[40] H. Alyousef, F. Aouaini, and M. Ben Yahia, "New insights on physico-chemical investigation of water adsorption isotherm into seed of dates using statistical physics treatment: pore size and energy distributions," *Journal of Molecular Liquids*, vol. 298, article 112041, 2020.

[41] B. Diu, C. Guthmann, D. Lederer, and B. Roulet, *Physique Statistique*, Hermann, Paris, 1989.

[42] M. Bouzid, Q. Zhu, D. M. Geoff, and A. Ben Lamine, "New insight in adsorption of pyridine on the two modified adsorbents types MN200 and MN500 by means of grand canonical ensemble," *Journal of Molecular Liquids*, vol. 263, pp. 413–421, 2018.

[43] L. D. T. Prola, E. Acayanka, E. C. Lima et al., "Comparison of Jatropha curcas shells in natural form and treated by non-thermal plasma as biosorbents for removal of reactive red 120 textile dye from aqueous solution," *Industrial Crops and Products*, vol. 46, pp. 328–340, 2013.

[44] D. W. Marquardt, "An algorithm for least-squares estimation of nonlinear parameters," *Journal of the Society for Industrial and Applied Mathematics*, vol. 11, no. 2, pp. 431–441, 1963.

[45] M. Hadi, M. R. Samarghandi, and G. McKay, "Equilibrium two-parameter isotherms of acid dyes sorption by activated carbons: study of residual errors," *Chemical Engineering Journal*, vol. 160, no. 2, pp. 408–416, 2010.

[46] T. V. Rêgo, T. R. S. Cadaval Jr., G. L. Dotto, and L. A. A. Pinto, "Statistical optimization, interaction analysis and desorption studies for the azo dyes adsorption onto chitosan films," *Journal of Colloid and Interface Science*, vol. 411, pp. 27–33, 2013.

[47] A. Kapoor and R. T. Yang, "Correlation of equilibrium adsorption data of condensible vapours on porous adsorbents," *Gas Separation and Purification*, vol. 3, no. 4, pp. 187–192, 1989.

[48] F. Aouaini, S. Knani, M. Ben Yahia, N. Bahloul, N. Kechaou, and A. Ben Lamine, "Application of statistical physics on the modeling of water vapor desorption isotherms," *Drying Technology*, vol. 32, no. 16, pp. 1905–1922, 2014.

[49] M. B. Yahia, F. Aouaini, M. Yahia, E. S. Almogait, and H. Al-Ghamdi, "Theoretical investigation of the chlorophyll nucleus adsorption monitored with quartz crystal microbalance technique: new insights on physicochemical properties," *Journal of Molecular Liquids*, vol. 289, article 111188, 2019.

[50] C. L. Sun and C. S. Wang, "Estimation on the intramolecular hydrogen-bonding energies in proteins and peptides by the analytic potential energy function," *Journal of Molecular Structure*, vol. 956, no. 1-3, pp. 38–43, 2010.

[51] B. von Oepen, W. Kördel, and W. Klein, "Sorption of nonpolar and polar compounds to soils: processes, measurements and experience with the applicability of the modified OECD-guideline 106," *Chemosphere*, vol. 22, no. 3-4, pp. 285–304, 1991.

[52] B. Yavorski and A. Detlaf, *Aide mémoire de Physique*, Edition Mir-Mouscou, Le-Livre (SABLONS, France), France, 1975.